PCCP

Molecular dynamics simulations of the lithium coordination environment in phosphate glasses†

Todd M. Alam,*[a] Jian-Jie Liang[b] and Randall T. Cygan[b]

[a] *Organic Materials Department, Sandia National Laboratories, MS-1407, Albuquerque, NM, 87185-1407, USA. E-mail: tmalam@sandia.gov*
[b] *Geochemistry Department, Sandia National Laboratories, MS-0750, Albuquerque, NM, 87185-0750, USA*

Received 9th June 2000, Accepted 15th August 2000
First published as an Advance Article on the web 15th September 2000

A molecular dynamics (MD) study of the lithium ultraphosphate glass series, $x\mathrm{Li_2O}\cdot(1-x)\mathrm{P_2O_5}$ ($0 \leqslant x \leqslant 0.5$) was used to investigate the changes in the Li environment with increasing modifier concentration. The results from the MD simulations indicate that only gradual structural variations in the Li coordination environment occur as a function of modifier content. Changes in the type of oxygen coordinated to the Li are observed to correlate with the minimum in the glass transition temperature. Additionally, changes in the number of shared phosphorus vertices were seen with increasing modifier concentration, in support of recent models involving the role of the cation modifier in the extended range structure of phosphate glasses. Empirical calculations of the ^{6}Li NMR chemical shifts directly from the MD simulation structures are also reported and compared to recent experimental solid-state NMR results.

1 Introduction

Phosphate glasses are technologically important materials, and are used in a variety of applications including glass-to-metal seals,[1] sealing frits,[2] nuclear waste forms,[3–5] lasers,[6–11] and optical components.[12] Understanding the relationship between the structure and the observed physical properties of phosphate glasses remains an area of active research. In many instances this structure–property correlation has not been realized. For example, in binary alkali ultraphosphate glasses a minimum in the glass transition temperature (T_g) is observed near the 20 to 25 mole percent alkali modifier concentration. Fig. 1 shows the T_g behavior for the $x\mathrm{Li_2O}\cdot(1-x)\mathrm{P_2O_5}$ glasses as a function of $\mathrm{Li_2O}$ concentration.[13,14] A similar analogous T_g minimum is not observed for silicate glasses.

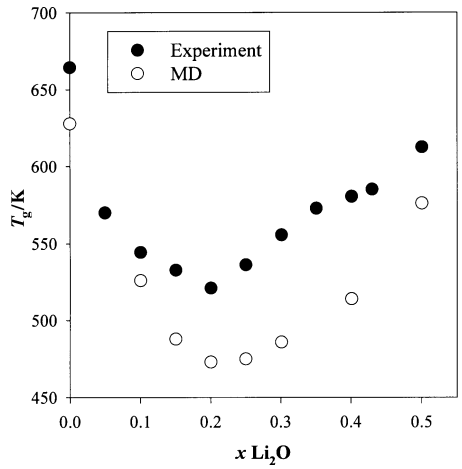

Fig. 1 Variation of the glass transition temperature (T_g) in the lithium ultraphosphate glass series, $x\mathrm{Li_2O}\cdot(1-x)\mathrm{P_2O_5}$ as a function of $\mathrm{Li_2O}$ concentration.

† Electronic Supplementary Information available. See http://www.rsc.org/suppdata/cp/b0/b004627m/

While there have been numerous experimental investigations into this anomalous T_g behavior in phosphate glasses, including NMR, Raman and XRD studies (see the recent reviews by Brow[15] and Hoppe,[16] plus references cited therein), an explanation of the structural changes responsible for the anomalous T_g minimum has yet to be confirmed.

Both theoretical *ab initio* and molecular dynamics (MD) investigations of phosphate glass structure have been reported. In contrast to the wealth of studies on silicate glass systems,[17–25] the number of theoretical investigations in phosphates has been limited, with the anisotropy of the phosphate bonding being a major complicating factor. The phosphorus atom contains five valence electrons, and yet maintains a tetrahedral hybridization such that the P–O bonds are intrinsically anisotropic. For example, in the single component $\mathrm{P_2O_5}$ glass this hybridization is clearly evident with three of the P–O bonds being bridging (with a P–O bond distance of 1.581 Å) along with a single terminal P=O bond (with a P–O distances of 1.432 Å).[26] The theoretical investigations to date show that for accurate simulations of phosphate materials the structural asymmetry of the P bonding must be reproduced, along with the ability to distinguish between P=O and P–O bonds. Uchino and co-workers have reported a series of *ab initio* orbital calculations on the electronic, structure and vibrational properties of alkali metaphosphate glasses.[27–29] MD simulations have been reported for the $\mathrm{NaPO_3}$,[30] $\mathrm{Mg(PO_3)_2}$, $\mathrm{Zn(PO_3)_2}$ and $\mathrm{Pb(PO_3)_2}$ glasses,[31,32] as well as the $x\mathrm{CaO}\cdot(1-x)\mathrm{P_2O_5}$,[33] $x\mathrm{Li_2O}\cdot(1-x)\mathrm{P_2O_5}$,[34] $0.5\mathrm{Na_2O}\cdot x\mathrm{Al_2O_3}\cdot(0.5-x)\mathrm{P_2O_5}$ and $(0.5-x/2)\mathrm{Na_2O}\cdot\mathrm{Al_2O_3}\cdot(0.5-x/2)\mathrm{P_2O_5}$ glass series.[35] The MD simulations reported by Liang *et al.*[34] for the ultraphosphate $x\mathrm{Li_2O}\cdot(1-x)\mathrm{P_2O_5}$ ($0 \leqslant x \leqslant 0.5$) glass system were the first theoretical study to directly address the question of the anomalous T_g behavior as a function of alkali modifier concentration in ultraphosphate glasses. In that initial report, the minimum in the T_g was replicated, along with a preliminary analysis of the structural variations that were observed with changing $\mathrm{Li_2O}$ concentration. It was demonstrated that the changes in the phosphate

ring structure correlated nicely with the T_g minimum, and that ring strain may play an important role in determining the glass properties.

Hoppe and co-workers[16,36,37] have recently presented evidence that the coordination and cross-linking of the alkali or alkaline earth cations used as backbone modifiers also play a significant role in the observed physical properties of phosphate glasses. In general, the initial addition of the modifying cation results in the depolymerization of the phosphate cross-linked network with breaking of the P–O–P bond and conversion of Q^3 to Q^2 units (in the Q^n terminology, n, denotes the number of P–O–P bonds in the phosphate tetrahedra).[38,39] This depolymerization process results in the initial observed decrease of T_g. At low modifier concentrations the cation is isolated and is coordinated by terminal oxygens (TO), both double bonded oxygens (DBO) and non-bridging oxygens (NBO). Above some critical concentration it is proposed that the TO are all coordinated to the metal cations, and that the metal coordination tetrahedra (MeO_n) begin to link. In this higher concentration range there is a reorganization of the glass network on the intermediate length scale resulting in an increasing T_g with modifier concentration. Hudgens and Martin[13] attribute this increase in network structure to the ability of the cations to form cross-links between adjacent phosphate chains. The effect of cross-linking of different phosphate rings by coordinating alkali cations is also supported by *ab initio* calculations on alkali metaphosphate glasses.[29] In the model forwarded by Hoppe and co-workers, structural reorganization of the glass network is predicted to occur when the cation coordination number (CN_{Me}) is equivalent to the number of terminal oxygens per modifying cation (M_{TO}). For glasses with the stoichiometry $x(Me_{2/v}O)\cdot(1-x)P_2O_5$, M_{TO} is defined by

$$M_{TO} = v(1/x) \tag{1}$$

where v is the metal (Me) valency. For the Li modifier, with a CN ~ 4–5,[40] the critical concentration is expected to occur for $x \sim 0.2$–0.25, corresponding nicely with the observed T_g minimum.

It is therefore important to investigate the role of the alkali environment on the phosphate glass structure as observed in MD simulations. In this manuscript we detail the variations in the Li cation environment observed in the MD simulation of the Li ultraphosphate series, $xLi_2O\cdot(1-x)P_2O_5$ ($0 \leqslant x \leqslant 0.5$). Correlation of this environment with the T_g minimum will be discussed. In addition, a comparison between recently reported ^{6}Li NMR results[40] and the Li chemical shifts empirically calculated from the simulated MD structures is presented.

2. Computational methods

2.1 MD simulations

The creation of a reliable force field to describe the interaction potentials involving phosphates is a very important step in the modeling of phosphate systems. The correct representation of the phosphate bonding anisotropy is important in the development of accurate models. For the MD simulations detailed here a forcefield model that explicitly incorporates both two- and three-body interactions was employed.[34] This model allows the P bonding asymmetry to be realized while treating all oxygen atoms identically. Partial charges instead of formal charges were used to describe the Coulombic (electrostatic) component of the system. In addition to the standard Coulombic interactions, a Lennard-Jones (LJ) potential function was used to describe the short-range two-body interactions:

$$E_{LJ} = D_0\left[\left(\frac{R_0}{r}\right)^{12} - 2\left(\frac{R_0}{r}\right)^{6}\right], \tag{2}$$

where r represents the interatomic distances, with R_0 and D_0 being adjustable parameters. For the LJ potential only cation–anion and anion–anion interactions make significant contributions to the overall energy, and were explicitly evaluated. The three-body energy terms were incorporated to describe both the O–P–O and P–O–P interactions, and are defined by

$$E_{angle} = \frac{k_0}{2}(\theta - \theta_0)^2, \tag{3}$$

where θ is either the O–P–O angle or the P–O–P angle, with adjustable parameters θ_0 and k_0. The partial charges and the forcefield potential parameters in eqn. (2) and (3) were determined by fitting the structure of crystalline lithium metaphosphate, $LiPO_3$ and the two orthorhombic phases of P_2O_5 as previously described,[34] and are summarized in Table 1.

MD simulations for eight compositions in the solid solution series, $xLi_2O\cdot(1-x)\ P_2O_5$, $x = 0.0$, 0.1, 0.15, 0.2, 0.25, 0.3, 0.4 and 0.5, were preformed using the CERIUS^2 software and the OFF energy program.[41] The MD simulations of the glasses were performed using a constant volume and temperature (NVT) canonical ensemble. For any given composition in the series, a rectangular simulation box containing 300–400 atoms was generated.[34] Details of the cell parameters are given in Table 1S of the supplementary material.† The compositions were equilibrated at 3000 K to achieve active melting for 50 ps, utilizing 1 fs time steps. Quenching of this equilibrated system from 3000 to 300 K was performed in 500 K intervals (the last step from 500 to 300 K), with each temperature step lasting 7 ps. This simulation sequence corresponds to a quench rate of $\sim 7.1 \times 10^{11}$ K s^{-1}. At 300 K, an additional 50 ps simulation was used to equilibrate the system.

The glass-transition (T_g) temperatures were determined by monitoring the volume–temperature relationship for a given composition in the MD simulations where the phosphate glass was treated as an NPT ensemble (constant pressure and temperature at each given temperature step) as previously described.[34] This computational approach is analogous to the experimental determination of T_g using dilatometry.

2.2 Calculation of ^{6}Li NMR chemical shifts

Koller *et al.*[42] has recently demonstrated that the observed NMR chemical shift of alkali species can be related to a chemical shift parameter A, where A is defined as the summation of the shift contributions for all the oxygens located within the first (and possibly the second) coordination sphere around the cation. For the present study of Li phosphate glasses, the chemical shift correlates directly to bond valence of the coordinating oxygen. An empirical bond valence (s_{ij}) between oxygen i and the cation j can be calculated from the cation–oxygen bond length, r_{ij}, using[43–45]

$$s_{ij} = \exp[(r_0 - r_{ij})/B] \tag{4}$$

where r_0 is the empirically derived oxygen–cation bond length of unit valence, and $B = 0.37$ is a constant previously

Table 1 Forcefield parameters for MD simulations[a]

Two-body interaction	D_0/eV	R_0/Å
$P^{1.85}$–$O^{-0.74}$	0.004 251	2.1550
$O^{-0.74}$–$O^{-0.74}$	0.012 185	3.2743
$Li^{0.37}$–$O^{-0.74}$	0.000 668	2.8890
Three-body interaction	k_0/eV rad^{-2}	θ_0/°
O–P–O	3.5401	109.47
P–O–P	20.9326	135.58

[a] See text and eqn. (2) and (3) for definitions of the symbols and parameters.

defined.[43–45] The total valence of the ith oxygen (W_i) is simply the summation over all oxygen–cation bond valences s_{ij} for each of the j cations bonded to the oxygens, including both lithium and phosphorous cations:

$$W_i = \sum_j s_{ij} \quad (5)$$

The chemical shift parameter A will then be a summation of the oxygen shift contributions with a $1/r_j^3$ (where r_i is the Li–O bond distance) distance dependence:

$$A = \sum_i \frac{W_i}{r_i^3} \quad (6)$$

The $1/r_i^3$ dependence was empirically obtained previously by Koller *et al.*[42] from fitting of model compounds. The resulting A values obtained from the MD simulations are given in Table 2. We recently reported an empirical linear relationship between the observed ^{6}Li chemical shift (δ) and the chemical shift parameter A for lithium phosphate systems,[40]

$$\delta(^6\text{Li}) = +4.30A - 5.85 \quad (7)$$

allowing the ^{6}Li chemical shift to be determined directly from the MD simulations.

3. Results

To address the performance of these MD forcefield potentials, the results of the simulations should be directly compared to the radial distribution functions, $G(r)$, obtained experimentally from X-ray and neutron diffraction studies of these glass compositions. Unfortunately, to the best of our knowledge diffraction studies for the lithium ultraphosphate glasses series has not been reported. The $G(r)$ obtained from a neutron diffraction[46] investigation of the lithium metaphosphate ($x = 0.5$) glass and a X-ray study[47] for a near metaphosphate glass composition ($x = 0.52$) are available, and are compared to the MD simulation for the $x = 0.5$ composition in Fig. 1S in the supplementary material.† The agreement between the MD simulation $G(r)$ and the neutron diffraction results[46] is very good, with the simulation slightly underestimating the P–O distance and distribution. The experimental X-ray and neutron $G(r)$ results are very different (See Fig. 1S in the supplementary material†), with the near metaphosphate glass composition showing a significantly broader distribution of radial distances. These variations may result from the different experimental techniques used to obtain the $G(r)$, as well as differences in the glass preparation and thermal history. The lack of experimental data for the entire lithium ultraphosphate composition series prevents a critical analysis of the MD potential performance, but the agreement at the metaphosphate composition is encouraging.

3.1 Li pair distribution functions

The variation of the Li environment for the phosphate glass series, $x\text{Li}_2\text{O}\cdot(1-x)\text{P}_2\text{O}_5$ ($0.1 \leqslant x \leqslant 0.5$) was determined by calculation of the Li pair distribution functions (PDF) for Li–O, Li–P and Li–Li at various Li_2O modifier concentrations for the MD simulations. The structural distances and average coordination numbers (CN) derived from the Li PDF plots (Fig. 2S–4S in the supplementary material†) are given in Tables 2 and 3.

The Li–O pair distribution functions (PDF) for different Li_2O concentrations are shown in Fig. 2S in the supplementary material.† The shape of the Li–O PDF shows little variation with increasing modifier concentration. The first peak for Li–O PDF ranges from 1.95 to 1.97 Å, with a full width at half maximum (FWHM) ranging from 0.32 to 0.35 Å. The first peak is asymmetric, tailing towards longer coordination distances. The Li–O PDF does not return to a null value after the first coordination sphere (see Fig. 2S), demonstrating that there is overlap between the first and second coordination shells. A similar result has been reported for the Na–O PDF

Table 2 Average coordination numbers and chemical shift parameters derived form the pair distribution functions in the $x\text{Li}_2\text{O}\cdot(1-x)\text{P}_2\text{O}_5$ glass series

Composition ($x\text{Li}_2\text{O}$)	CN[a]			A^b	δ ^{6}Li (ppm)[c]
	Li–O (3.0 Å)	Li–P (4.5 Å)	Li–Li (6.0 Å)		
0.10	4.7	7.2	1.6	0.99	−1.59
0.15	4.5	7.4	2.9	0.97	−1.68
0.20	4.2	6.7	4.3	1.00	−1.55
0.25	4.6	6.7	4.1	1.01	−1.51
0.30	4.4	7.0	6.6	1.08	−1.21
0.40	5.0	6.7	9.7	1.07	−1.25
0.50	5.1	6.5	14.2	1.12	−1.03

[a] CN = Average coordination number. The cutoff distance (in Å) used in the calculation of CN is shown in parentheses. [b] Chemical shift parameter as defined in eqn. (6). [c] Chemical shift calculated using the empirical relationship in eqn. (7).

Table 3 Structural distances derived from the pair distribution functions in the $x\text{Li}_2\text{O}\cdot(1-x)\text{P}_2\text{O}_5$ glass series

Composition ($x\text{Li}_2\text{O}$)	1st peak/Å			2nd peak/Å			
	Li–Li	Li–P	Li–O	Li–O	⟨Li–O⟩ (3.0 Å)[a]	⟨Li–P⟩ (4.5 Å)[a]	⟨Li–Li⟩ (6.0 Å)[a]
0.10	2.45	3.25	1.97	4.27	2.27	3.78	4.05
0.15	2.79	3.27	1.95	4.29	2.26	3.75	4.88
0.20	2.91	3.23	1.95	4.29	2.18	3.68	4.66
0.25	2.69	3.27	1.97	4.29	2.27	3.67	4.27
0.30	2.93	3.27	1.95	4.27	2.20	3.63	4.51
0.40	2.83	3.25	1.95	4.31	2.27	3.63	4.55
0.50	2.83	3.25	1.97	4.31	2.25	3.53	4.67

[a] The cutoff distance (in Å) used in the calculation of the average coordination distance is shown in parentheses.

in the MD simulation of $NaPO_3$ glass.[30] Because of this coordination sphere overlap, it is important to include the cut-off distances used in the determination of structural parameters, including average bond lengths and CN. Variations in the cut-off distance have a dramatic effect on the resultant values. Due to this asymmetry and coordination sphere overlap an average Li–O distance using a 3.0 Å cutoff is also reported (Table 2). The average Li–O distance of 2.25 Å for the metaphosphate composition ($x = 0.5$) is longer than the 2.03 Å reported in the neutron diffraction study of $LiPO_3$ glass,[47,48] or the average 1.96 Å Li–O bond distance observed for crystalline $LiPO_3$. The second peak in the Li–O PDF, along with the average Li–O CN as a function of Li_2O concentration are given in Tables 2 and 3. The average CN ranges between 4 and 5, and is consistent with experimental estimations of CN.[40,47,48]

The Li–P PDF as a function of Li_2O concentration is shown in Fig. 3S of the supplementary material,† with the first coordination peak varying between 3.25 and 3.27 Å and a FWHM between 0.5 and 0.63 Å. The second coordination peak is very broad and asymmetric, such that the peak position was not reliably determined. The shape of the Li–P PDF is unchanged with increasing Li_2O concentration. The average Li–P bond length calculated using a 4.5 Å cutoff was found to decrease gradually with increasing modifier concentration, and reflects the change in the valency of the coordinated oxygen in the Li–O–P bond (see discussion below). The average Li–P CN varied between 6.5 and 7.4 (see Table 2), but did not show any clear trends.

The Li–Li PDF is shown in Fig. 4S of the supplementary material,† and reveals a very broad and asymmetric peak that varies between 2.45 and 2.93 Å, having a FWHM peak width ranging between ~0.5 to 1.5 Å. The average Li–Li distance using a 6 Å cutoff varied between 4.05 and 4.88 Å. The average Li–Li CN steadily increases between 1.6 and 14.2 between $x = 0.1$ and 0.5. For $x > 0.1$ the Li–Li PDF shows significant tailing for Li–Li distances greater than 4 Å. The $x = 0.1$ PDF is shifted to slightly smaller Li–Li distance, and does not appear to have as many long range Li–Li distances present within the PDF. While these may suggest shorter Li–Li interactions at very low Li_2O concentrations, the very low average Li–Li CN (Table 2) shows that initially the Li cations are relatively isolated. The broad nature of the Li–Li PDF strongly suggests that the Li cations are randomly distributed throughout the glass network for the entire ultraphosphate concentration regime.

3.2 Coordination environment

To address the change in the oxygen type that is coordinated to the Li with variation of the Li_2O concentration, selected P–O PDF for $x = 0.1$, 0.25 and 0.4 are shown in Fig. 2a, while Fig. 2b shows the average P–O bond distance for oxygens that are within the first coordination sphere of the Li (cutoff distance 3.0 Å). The minimum P–O distance for each coordinating oxygen was used to determine the average shown in Fig. 2b, and only includes oxygens that are coordinating in the average. In Fig. 2a the different P–O bond distances are clearly evident in the simulated P–O PDF. The TO P–O bond distance (both NBO and DBO) is approximately 1.45 Å with the BO P–O distance being approximately 1.53 Å. There is a very small increase in the TO and BO P–O bond lengths with the addition of Li_2O (1.47 and 1.57 Å, respectively at $x = 0.5$). These results compare to the experimental 1.43 Å terminal DBO P–O bond length, and a 1.58 Å BO P–O bond distance observed for vitreous P_2O_5.[26] In crystalline $LiPO_3$, the NBO P–O distance is 1.44 Å, with the BO P–O distance being 1.6 Å. Lengthening of the P–O bond length with increasing modifier content has been observed experimentally in ultraphosphate glasses,[26] and is of similar magnitude to that observed in the MD simulations (see Fig. 5 of ref. 26). The relative

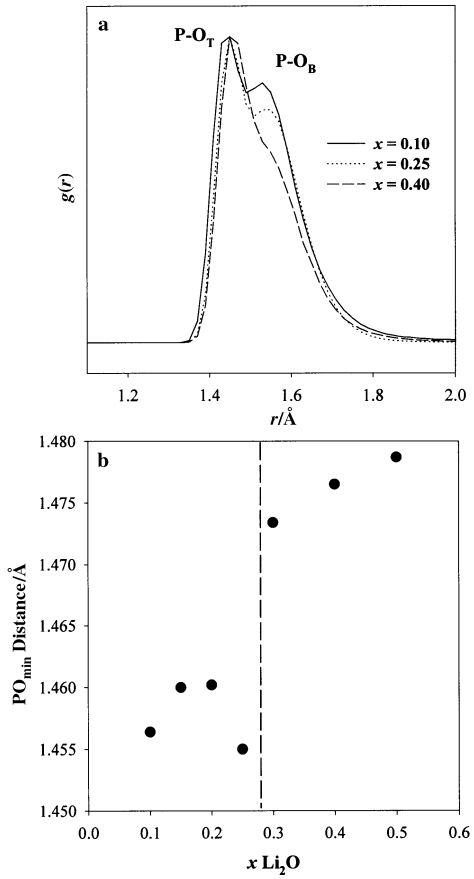

Fig. 2 (a) Select P–O pair distribution function, $g(r)$, for the $xLi_2O \cdot (1 - x)P_2O_5$ glass for different Li_2O concentrations, and (b) variation of the average minimum P–O bond distance for oxygens within the 3.5 Å coordination sphere of Li obtained from MD simulations as a function of Li_2O concentration.

amount of BO also decreases with increasing Li_2O concentration as predicted due to depolymerization of the phosphate network.

By determining the minimum P–O bond distance for oxygens in the Li coordination sphere (Fig. 2b), the type of coordinating oxygen can be addressed. In the MD simulations this average P–O distance ranges from 1.455 to 1.480 Å between $x = 0.1$ and 0.5. This average is similar to the average TO P–O bond distance observed for the entire glass series (see Fig. 2a). This clearly demonstrates that BO oxygens do not play an important role in the coordination of the Li modifier, and that the first coordination sphere around Li is predominantly TO.

Fig. 3 shows the variation of the average number of Li surrounding a phosphorus atom as a function of Li_2O concentration. A cutoff distance of 4.5 Å was utilized, and only CN for phosphorus that actually have Li within this coordination sphere were utilized in calculation of the average CN. At $x = 0.1$ this P–Li CN is ~1.5 suggesting that on average the Li do not significantly share P vertices. This coordination increases steadily with higher Li_2O concentration, with a distinct change in the variation occurring near $x = 0.25$.

3.3 ^{6}Li NMR chemical shifts

In order to compare the structural information about the Li environment derived from MD simulations to experimentally observed NMR results, the ^{6}Li chemical shifts were calculated directly from the MD structures. The ^{6}Li NMR chemical shift is expected to be sensitive to variations in the local Li coordination environment, and should reflect any changes in the Li PDF. Using eqn. (4)–(7) the average ^{6}Li chemical shift was

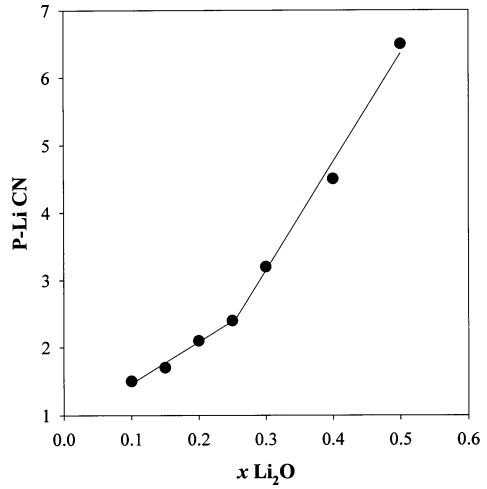

Fig. 3 Variation in the average number of Li cations within the local environment of P as a function of Li_2O concentration obtained from MD simulations. Only those P with Li within 4.5 Å are considered in the average.

calculated from the MD structures as a function of Li_2O concentration and are given in Table 2 and Fig. 4. The intercept of this line can be adjusted by variation in the cutoff distance used in the calculation of the A parameter. For example, increasing the cutoff distance to include values >3.5 Å will increase A and similarly δ through eqn. (6) and (7). It is possible to increase this cutoff distance to provide an improved fit between the experimental and the MD calculated chemical shifts. For the present discussion a 3.5 Å cutoff distance was utilized, as this was the original cutoff distance used in the development of the empirical relationship in eqn. (7).[40]

4. Discussion

These MD simulations show that in general there are only small variations of the Li environment with increasing Li_2O concentration. In particular, there are no major structural changes in the Li coordination environment that would correlate with the T_g minimum observed in Fig. 1. This is in contrast to the observation of major changes in the phosphate ring structure as a function of modifier concentration previously reported for this, $xLi_2O \cdot (1-x)P_2O_5$ ($0.1 \leqslant x \leqslant 0.5$) glass series.[34]

The MD simulations presented here do reveal subtle variations in the Li coordination environment that are consistent with the modifier restructuring model forwarded by Hoppe and co-workers.[16,36,37,49] A schematic illustration of this model is shown in Fig. 5, for low, medium and high modifier concentrations. As seen in Fig. 2b there is a step in the average minimum P–O bond distance for concentrations $x > 0.25$, signaling a change in the coordinating oxygen type. It is expected that the average TO P–O bond would show a linear lengthening with increasing modifier content,[26] such that a random distribution of DBO and NBO in the Li coordination sphere would result in a linear variation of the minimum P–O bond distance. The step in the minimum P–O bond distance of coordinating oxygens fits well with the pictorial representation of the Hoppe modifier restructuring model where the initial coordination involves both DBO and NBO in isolated LiO_n polyhedra. At the critical concentration the number of TO available is equal to the CN [M_{TO}, eqn. (1)], such that any additional increase in the Li_2O concentration will require LiO_n polyhedra to link together by corner and edges. This linking of polyhedra would be expected to manifest itself in the lengthening of the average coordinating P–O bond length, as the electron density shifts along the P–O bond to charge compensate the charge of the shared modifier sites.[26]

The low number of Li coordinating to a given phosphorus atom (Fig. 3), along with the low Li–Li CN (Table 2) show that initially the Li cations are relatively isolated (CN ~ 1.5). Above the critical concentration of $x \sim 0.25$, the average coordination of Li around a phosphorus increases dramatically, consistent with edge and corner sharing. The increase in the average Li–Li CN (Table 2) is consistent with the formation of O–Li–O cross-links between neighboring phosphorus tetrahedra, but an increase in the Li–Li CN is also expected to result from increases in the Li number density.

The MD simulations also provide insight into the surprising linear behavior of the ^{6}Li MAS NMR chemical shifts. From eqn. (6) changes in the Li–O CN would be expected to produce a variation in the chemical shift, yet the observed ^{6}Li NMR chemical shift is essentially linear for $0.05 \leqslant x \leqslant 0.5$. From Table 3 we can see that there is a minimum in Li–O CN

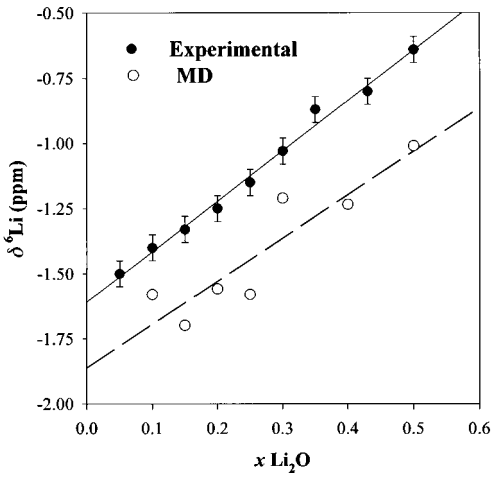

Fig. 4 Variation of the ^{6}Li NMR chemical shift as a function of Li_2O concentration, (●) experimental and (○) predicted from MD simulations.

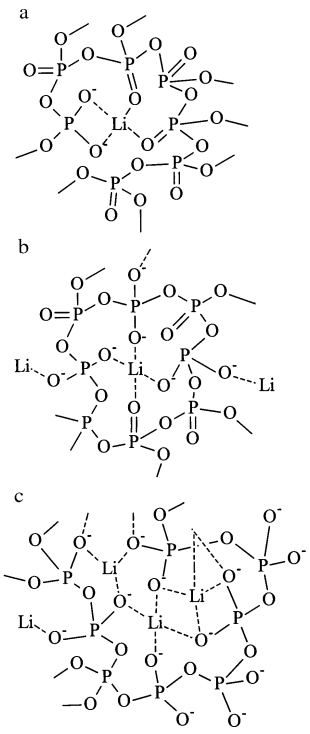

Fig. 5 A schematic illustration of the changes in the Li environment in lithium ultraphosphate glasses for different Li_2O concentration regimes: (a) low, (b) medium and (c) high. Adapted from ref. 40.

at $x \sim 0.2$, which should result in a minimum in the magnitude of the shift parameter A and subsequently a minimum in the chemical shift [eqn. (7)]. Inspection of Table 2 shows that there is also a variation of the Li–O bond distance with a minimum near $x \sim 0.2$, which maximizes the shift parameter A. The combination of these two non-linear effects tends to balance out to produce the observed linear behavior. This observation demonstrates the NMR analysis of alkali chemical shifts may not reveal subtle changes in the coordination environment, since the shift depends on the combination of several different variables describing the coordination environment.

The results of the MD simulations also agree with recent NMR ^{7}Li–^{31}P and ^{31}P–^{7}Li rotational-echo double resonance (REDOR) MAS experiments.[50] REDOR experiments allow a measure of the dipolar coupling between different nuclei, and thus a measure of spatial proximity. REDOR experiments on Li phosphate glasses have shown that the dipolar coupling between Li and P is rather independent of the Li_2O concentration, demonstrating that the P environment around a Li cation is unchanged. The MD simulations (Tables 2 and 3) predict a similar behavior since the average Li–P distance is constant, and the average Li–P CN shows only a small variation. The REDOR experiments also demonstrate that the Li environment around a P changes distinctly near $x \sim 0.25$. This experimental observation may correspond to the change in slope noted in the average P–Li CN (Fig. 3) obtained for the MD simulations. A more future analysis of these REDOR results is warranted.

The MD simulations demonstrate that while there are changes in the Li environment that do correlate with the observed T_g minimum, the effects or changes are more gradual that one would predict from the simplified cation restructuring model defined by eqn. (1) and schematically detailed in Fig. 5. A gradual variation of the coordination environments with changes in modifier concentration would appear to be more realistic than a sudden and distinct environmental change. Whether the anomalous T_g in alkali ultraphosphate glasses is produced solely by these Li environment changes, results from the formation of phosphate ring structures[34] (still not experimentally verified), or is a combination of these two effects remains to be determined. Further comparison between MD simulations and experimental results in phosphate glass systems are presently being pursued.

Acknowledgements

This work was supported by the Basic Energy Science (BES) program at Sandia National Laboratories. Sandia is a multiprogram laboratory operated by Sandia Corporation, a Lockheed Martin Company, for the United States Department of Energy under Contract DE-AC04-94AL85000. The authors would like to thank J. Swenson for providing a copy of the experimental neutron diffraction pair distribution function of the lithium metaphosphate glass.

References

1 J. A. Wilder, *J. Non-Cryst. Solids*, 1980, **38–39**, 879.
2 R. Morena, *J. Non-Cryst. Solids*, 2000, **263–264**, 382.
3 D. E. Day, Z. Wu, C. S. Ray and P. Hrma, *J. Non-Cryst. Solids*, 1998, **241**, 1.
4 S. V. Raman, *J. Non-Cryst. Solids*, 2000, **263–264**, 395.
5 X. Fang, C. S. Ray, G. K. Marasinghe and D. E. Day, *J. Non-Cryst. Solids*, 2000, **263–264**, 293.
6 T. Härig, G. Huber and I. A. Shcherbakov, *J. Appl. Phys.*, 1981, **52**, 4450.
7 M. J. Weber, *J. Non-Cryst. Solids*, 1990, **123**, 208.
8 S. A. Payne, M. L. Elder, J. H. Cambell, G. D. Wilke, M. J. Weber and Y. T. Hayden, *Ceram. Trans.*, 1992, **28**, 253.
9 J. H. Cambell and T. I. Suratwala, *J. Non-Cryst. Solids*, 2000, **263–264**, 318.
10 D. L. Veasey, D. S. Funk, P. M. Peters, N. A. Sanford, G. E. Obarski, N. Fontaine, M. Young, A. P. Peskin, W.-C. Liu, S. N. Houde-Walter and J. S. Hayden, *J. Non-Cryst. Solids*, 2000, **263–264**, 369.
11 P. R. Ehrmann, J. H. Cambell, T. I. Suratwala, J. S. Hayden, D. Krashkevich and K. Takeuchi, *J. Non-Cryst Solids*, 2000, **263–264**, 251.
12 S. Jiang, T. Luo, B.-C. Hwang, F. Smekatala, K. Seneschal, J. Lucas and N. Peyghambarian, *J. Non-Cryst. Solids*, 2000, **263–264**, 364.
13 J. J. Hudgens and S. W. Martin, *J. Am. Ceram. Soc.*, 1993, **76**, 1691.
14 J. J. Hudgens, R. K. Brow, D. R. Tallant and S. W. Martin, *J. Non-Cryst. Solids*, 1998, **223**, 21.
15 R. K. Brow, *J. Non-Cryst. Solids*, 2000, **263–264**, 1.
16 U. Hoppe, *J. Non-Cryst. Solids*, 2000, **263–264**, 29.
17 F. L. Galeener, *J. Non-Cryst. Solids*, 1982, **49**, 53.
18 C. Huang and A. N. Cormack, *J. Chem. Phys.*, 1990, **93**, 8180.
19 B. Vessal, *J. Non-Cryst. Solids*, 1994, **177**, 103.
20 Y. Benino, K. Hirao and N. Soga, *J. Non-Cryst. Solids*, 1995, **183**, 22.
21 J. Habasaki, I. Okada and Y. Hiwatari, *J. Non-Cryst. Solids*, 1995, **183**, 12.
22 T. Peres, D. A. Litton, J. A. Capobianco and S. H. Garofalini, *J. Non-Cryst. Solids*, 1997, **221**, 34.
23 T. Uchino, Y. Tokuda and T. Yoko, *Phys. Rev. B*, 1998, **58**, 5322.
24 B. Park and A. N. Cormack, *J. Non-Cryst. Solids*, 1999, **255**, 112.
25 N. T. Huff, E. Demiralp, T. Cagin and W. A. Goddard, *J. Non-Cryst. Solids*, 1999, **253**, 133.
26 U. Hoppe, R. Kranold, D. Stachel, A. Barz and A. C. Hannon, *Z. Naturforsch., A*, 2000, **55**, 369.
27 T. Uchino and Y. Ogata, *J. Non-Cryst. Solids*, 1995, **181**, 175.
28 T. Uchino and Y. Ogata, *J. Non-Cryst. Solids*, 1995, **191**, 56.
29 T. Uchino and T. Yoko, *J. Non-Cryst. Solids*, 2000, **263–264**, 180.
30 A. Speghini, E. Sourial, T. Peres, G. Pinna, M. Bettinelli and J. A. Capobianco, *Phys. Chem. Chem. Phys.*, 1999, **1**, 173.
31 G. Cormier, J. A. Capobianco and A. Monteil, *J. Non-Cryst. Solids*, 1994, **168**, 115.
32 E. Sourial, T. Peres, J. A. Capobianco, A. Speghini and M. Bettinelli, *Phys. Chem. Chem. Phys.*, 1999, **1**, 2013.
33 D. K. Belashchenko, *Inorg. Mater.*, 1997, **33**, 475.
34 J.-J. Liang, R. T. Cygan and T. M. Alam, *J. Non-Cryst. Solids*, 2000, **263–264**, 167.
35 H. Inoue, A. Makishima, T. Kanazawa, T. Nanba and I. Yusai, *Phys. Chem. Glasses*, 1995, **36**, 37.
36 U. Hoppe, G. Walter, R. Kranold, D. Stachel and A. Barz, *J. Non-Cryst. Solids*, 1995, **192–193**, 28.
37 U. Hoppe, *J. Non-Cryst. Solids*, 1996, **195**, 138.
38 R. J. Kirkpatrick and R. K. Brow, *Solid State Nucl. Magn. Reson.*, 1995, **5**, 9.
39 R. K. Brow, D. R. Tallant, J. J. Hudgens, S. W. Martin and A. D. Irwin, *J. Non-Cryst. Solids*, 1994, **177**, 221.
40 T. M. Alam, S. Conzone, R. K. Brow and T. J. Boyle, *J. Non-Cryst. Solids*, 1999, **258**, 140.
41 The MD simulations were performed using the CERIUS2 software package and the OFF energy program, Molecular Simulations Inc., 2000.
42 H. Koller, G. Engelhardt, A. P. M. Kentegens and J. Sauer, *J. Phys. Chem.*, 1994, **98**, 1544.
43 I. D. Brown and R. D. Shannon, *Acta Crystallogr., Sect. A*, 1973, **29**, 266.
44 I. D. Brown and D. Altermatt, *Acta Crystallogr., Sect. B*, 1985, **41**, 244.
45 N. E. Brese and M. O'Keefee, *Acta Crystallogr., Sect. B*, 1991, **47**, 192.
46 J. Swenson, A. Matic, A. Brodin, L. Börjesson and W. S. Howells, *Phys. Rev. B*, 1998, **58**, 11331.
47 K. Muruganandam, M. Seshasayee and S. Patnaik, *Solid State Ionics*, 1996, **89**, 313.
48 J. Swenson, A. Matic, A. Brodin, L. Börjesson and W. S. Howells, *Phys. Rev. B*, 1998, **58**, 11331.
49 U. Hoppe, G. Walter, D. Stachel, A. Barz and A. C. Hannon, *Z. Naturforsch., A*, 1997, **52**, 259.
50 L. Van Wullen, H. Eckert and G. Schwering, *Chem. Mater.*, 2000, **12**, 1840.